Spin and orbital magnetisation densities determined by Compton scattering of photons

1990 J. Phys.: Condens. Matter 2 6439

(http://iopscience.iop.org/0953-8984/2/30/009)

J. Phys.: Condens. Matter 2 (1990) 6439–6449. Printed in the UK

Spin and orbital magnetisation densities determined by Compton scattering of photons

S P Collins†, M J Cooper‡, S W Lovesey§‖ and D Laundy†
† Daresbury Laboratory, Warrington WA4 4AD, UK
‡ Department of Physics, University of Warwick, Coventry CV4 7AL, UK
§ Rutherford Appleton Laboratory, Chilton, Oxon OX11 0QX, UK
‖ Institute of Physics, University of Uppsala, S-75121 Uppsala, Sweden

Received 14 February 1990

Abstract. Compton scattering of a circularly polarised photon beam is shown to provide direct information on orbital and spin magnetisation densities. Experiments are reported which demonstrate the feasibility of the method by correctly predicting the ratio of spin to orbital magnetisation components in iron and cobalt. A partially polarised beam of 45 keV photons from the Daresbury Synchrotron Radiation Source produces charge–magnetic interference scattering which is measured by a field-difference method. Theory shows that the interference cross section contains the Compton profile of polarised electrons modulated by a structure factor which is a weighted sum of spin and orbital magnetisations. In particular, the scattering geometry for which the structure factor vanishes yields a unique value for the ratio of the magnetisation densities. Compton scattering, being an incoherent process, provides data on total unit-cell magnetisations which can be directly compared with bulk data. In this respect, Compton scattering complements magnetic neutron and photon Bragg diffraction.

1. Introduction

It has been recognised for some time that magnetic photon Bragg diffraction has an advantage over neutron diffraction inasmuch as it can be used to separately determine spin and orbital magnetisation densities in solids (for reviews see, e.g., de Bergevin and Brunel 1986, Cooper 1987). This has already been exploited in diffraction studies of antiferromagnets such as holmium where the weak magnetic reflections are separate from the Bragg peaks (Gibbs *et al* 1988); the situation is more difficult in ferromagnets where charge and magnetic peaks are superimposed. Here, we point out that the Compton limit of high-energy photon scattering, which is inelastic and incoherent, also provides a direct method of separating spin and orbital densities in ferromagnets. We report the first observations at the Synchrotron Radiation Source (SRS) facility, Daresbury, using, as examples, metallic ferromagnets.

The success of the experiments reported hinges on the observation that charge–magnetic interference induced by circular polarisation is a weighted sum of spin and orbital magnetisations and vanishes for a particular scattering geometry. The interference term is isolated in the scattering intensity from the (dominant) pure charge and pure magnetic contributions by switching the polarity of a field applied to the sample

0953-8984/90/306439 + 11 $03.50

and recording the difference signal. The angles that define the configuration at which the signal vanishes are obtained by fitting data sets recorded as a function of the orientation of the magnetic field relative to the incident beam, the incident and scattered beam directions being fixed. From a knowledge of the vanishing point a unique value for the ratio of the spin to orbital magnetisation densities is obtained.

In magnetic photon diffraction from solids the magnetic information is in Bragg peaks. Unfortunately, the structure factor limits the number of peaks that can be measured since it vanishes in the forward direction and at large scattering vectors. Compton scattering is shown to provide information on the total spin and orbital unit-cell magnetisations which directly relates to bulk magnetisation measurements. In this respect, Compton scattering is different from photon and neutron diffraction, but the various data sets are clearly complementary.

Magnetic neutron diffraction data for atomic form factors do not usually extrapolate smoothly to a value in accord with the measured bulk magnetic moment (Moon 1986). Data on metallic ferromagnets are consistent with a spin form factor, normalised to unity in the forward direction, scaled by a factor $1 + \alpha$, where α is typically about 0.20. The physical interpretation of α is the subject of debate, but an appealing picture is that it arises from an essentially uniform background of negative magnetisation induced in conduction electrons. In any event, this component of the magnetisation density is more or less uniform in space. Hence, in a diffraction pattern it appears in the forward direction and it is absent in observed Bragg peaks. However, a uniform magnetisation is contained in the Compton scattering data because it relates to the bulk magnetisation density and its association with low-momentum electrons is confirmed in the magnetic Compton profile (Cooper *et al* 1988, Collins *et al* 1989).

Our theoretical material is presented in the next two sections, which are followed by a description of the experiment and findings for metallic ferromagnets. In the first theoretical section we discuss the cross section for scattering a circularly polarised photon beam from a magnetic material and report the form of the amplitude appropriate far from any resonance events. The charge–magnetic interference term induced by circular polarisation can be observed by a magnetic field difference technique, for example. The derivation of the Compton limit of the cross section is taken up in section 3. The experimental set-up, described in section 4, is similar to that adopted for magnetic Compton measurements (Collins *et al* 1989). The analysis of data for iron and cobalt is described in section 5 and conclusions are gathered in section 6.

2. Photon cross section

We begin by recording a compact expression for the non-relativistic partial differential cross section in terms of a correlation function formed with the scattering amplitude operator. Let $E = \hbar cq$ and $E' = \hbar cq'$ denote the energies of the incident and scattered photons. The changes in wavevector and energy in the scattering process are $\boldsymbol{k} = \boldsymbol{q} - \boldsymbol{q}'$ and $\hbar\omega = E - E'$, respectively. The polarisation states are described in terms of a density matrix $\boldsymbol{\mu}$, defined in accord with Balcar and Lovesey (1989), and $\mathbf{G}(\boldsymbol{k})$ denotes the scattering amplitude whose explicit form, in terms of polarisation vectors and atomic

quantities, is given later in the section. With these definitions the cross section for scattering into an element $d\Omega$ of solid angle is

$$\frac{d^2\sigma}{d\Omega\, dE'} = r_e^2 \frac{E'}{E} \int_{-\infty}^{\infty} \frac{dt}{2\pi\hbar} \exp(-i\omega t)\, \mathrm{Tr}[\boldsymbol{\mu}\langle \mathbf{G}^+(\boldsymbol{k})\mathbf{G}(\boldsymbol{k}, t)\rangle]. \tag{2.1}$$

Here, r_e is the classical electron radius, the trace operation is with respect to polarisation states and $\langle \ldots \rangle$ denotes the thermal average of the enclosed quantity. The Heisenberg operator $\mathbf{G}(\boldsymbol{k}, t)$, in which t has the dimension of time, is formed in the standard manner; the definition is used in the following section.

An expression for $\mathbf{G}(\boldsymbol{k})$ is obtained from the work of Grotch *et al* (1983). We represent it in terms of a 2×2 matrix notation for plane polarisation states, defined with polarisation vectors $\boldsymbol{e}, \boldsymbol{e}'$ using the scheme displayed in figure 6.2 of Balcar and Lovesey (1989). The expression for $\mathbf{G}(\boldsymbol{k})$ given there is recovered from the following expression in the elastic limit $\omega = 0$. The expression, which encompasses inelastic events, is found to be

$$\mathbf{G}(\boldsymbol{k}) = n(\boldsymbol{k})\boldsymbol{e}' \cdot \boldsymbol{e} - ig[\boldsymbol{S}(\boldsymbol{k}) \cdot \mathbf{B} + \boldsymbol{Z}(\boldsymbol{k}) \cdot (\boldsymbol{e}' \times \boldsymbol{e})] \tag{2.2}$$

where $g = E/m_e c^2$. This result is obtained from a perturbation expansion in g which in the work reported here is 45/510 and thus small enough to ensure the soundness of equation (2.2) as the basis of an interpretation. Using the notations $b = E'/E$, $a = (1 + b)/2$, $\hat{\boldsymbol{q}} = \boldsymbol{q}/q$ and similarly for the unit vector $\hat{\boldsymbol{q}}'$,

$$\mathbf{B} = \begin{pmatrix} a(\hat{\boldsymbol{q}} \times \hat{\boldsymbol{q}}') & (a-b)\hat{\boldsymbol{q}} - (a - b\cos\theta)\hat{\boldsymbol{q}}' \\ (a - \cos\theta)\hat{\boldsymbol{q}} + (1-a)\hat{\boldsymbol{q}}' & (b + 1 - a)(\hat{\boldsymbol{q}} \times \boldsymbol{q}') \end{pmatrix}. \tag{2.3}$$

The angle between $\hat{\boldsymbol{q}}$ and $\hat{\boldsymbol{q}}'$ is denoted by θ in this expression.

The atomic quantities in (2.2) involve the position $\boldsymbol{R}_j$, spin $\boldsymbol{s}_j$ and momentum $\boldsymbol{p}_j$ of the electron labelled j. The spatial Fourier transforms of the charge and spin-density operators are

$$n(\boldsymbol{k}) = \sum_j \exp(i\boldsymbol{k} \cdot \boldsymbol{R}_j) \tag{2.4}$$

and

$$\boldsymbol{S}(\boldsymbol{k}) = \sum_j \exp(i\boldsymbol{k} \cdot \boldsymbol{R}_j)\, \boldsymbol{s}_j = \frac{-1}{2\mu_B} \int d\boldsymbol{r} \exp(i\boldsymbol{k} \cdot \boldsymbol{r})\, \boldsymbol{M}_s(\boldsymbol{r}) \tag{2.5}$$

while

$$\boldsymbol{z}(\boldsymbol{k}) = \frac{i}{\hbar q^2} \sum_j \exp(i\boldsymbol{k} \cdot \boldsymbol{R}_j)\, (\boldsymbol{q} - \boldsymbol{q}'/b) \times \boldsymbol{p}_j \tag{2.6}$$

will be shown to be related to the orbital angular momentum density $\boldsymbol{M}_L(\boldsymbol{r})$.

The various terms in the cross section (2.1) can be generated from (2.2) and (2.3) using the method employed by Balcar and Lovesey (1989). Here the charge–magnetic interference term induced by circular polarisation in the incident photon beam is of particular interest. This component of $\mathrm{Tr}[\boldsymbol{\mu}\mathbf{G}^+(\boldsymbol{k})\mathbf{G}(\boldsymbol{k})]$ is readily shown to be

$$gn^+(\boldsymbol{k})P_2[\![-\boldsymbol{S}(\boldsymbol{k}) \cdot \{(1 - \cos\boldsymbol{\theta})(\hat{\boldsymbol{q}}\cos\theta + \hat{\boldsymbol{q}}') + (\varepsilon/2)[\hat{\boldsymbol{q}}(1 + \cos\theta) + \hat{\boldsymbol{q}}'(1 - 3\cos\theta)]\} + \boldsymbol{z}(\boldsymbol{k}) \cdot (\hat{\boldsymbol{q}} + \hat{\boldsymbol{q}}'\cos\theta)]\!] \tag{2.7}$$

where $\varepsilon = E'/E - 1 = -\hbar\omega/E$ and P_2 is the component of the Stokes vector that describes circular polarisation. Some algebra is necessary to establish the result

$$\boldsymbol{Z}(\boldsymbol{k}) \cdot (\boldsymbol{q} + \boldsymbol{q}' \cos\theta) = \{[-(1+\cos\theta)k^2]/[q^2(2+\varepsilon)]\}\boldsymbol{T}_L(\boldsymbol{k}) \cdot (\hat{\boldsymbol{q}} + \hat{\boldsymbol{q}}') \tag{2.8}$$

in which the orbital angular momentum operator

$$\boldsymbol{T}_L(\boldsymbol{k}) = \frac{-\mathrm{i}}{\hbar k^2} \sum_j \exp(\mathrm{i}\boldsymbol{k} \cdot \boldsymbol{R}_j)(\boldsymbol{k} \times \boldsymbol{p}_j) = \frac{-1}{2\mu_B} \int \mathrm{d}\boldsymbol{r} \exp(\mathrm{i}\boldsymbol{k} \cdot \boldsymbol{r})\hat{\boldsymbol{k}} \times [\boldsymbol{M}_L(\boldsymbol{r}) \times \hat{\boldsymbol{k}}]\}. \tag{2.9}$$

In the limit of elastic scattering $\varepsilon = 0$ and the result (2.7) with (2.8) reduces to the corresponding result given by Balcar and Lovesey (1989). Note that the magnetic density equals $\boldsymbol{M}_S = \boldsymbol{M}_L$.

Finally we give the form of (2.7) for the scattering geometry in which the spin and orbital densities $\boldsymbol{M}_S$ and $\boldsymbol{M}_L$ are aligned by a magnetic field that is at an angle α to the incident beam, as illustrated in figure 1. We find that

$$\begin{aligned}\frac{gn^+(\boldsymbol{k})P_2}{2\mu_B} \int \mathrm{d}\boldsymbol{r} \exp(\mathrm{i}\boldsymbol{k} \cdot \boldsymbol{r}) \llbracket M_S(\boldsymbol{r})\{(1-\cos\theta)(2\cos\theta\cos\alpha \\ + \sin\theta\sin\alpha) + (\varepsilon/2)\,[\cos\alpha(1+3\cos\theta)(1-\cos\theta) \\ + \sin\theta\sin\alpha\,(1-3\cos\theta)]\} + M_L(\boldsymbol{r})\,[\sin\theta(1+\cos\theta)/2(2+\varepsilon)] \\ \times \{4\sin(\tfrac{1}{2}\theta)\cos(\alpha-\tfrac{1}{2}\theta) + \varepsilon[\sin\alpha + (3+\varepsilon)\sin(\theta-\alpha)]\}\rrbracket \\ = \frac{n^+(\boldsymbol{k})}{\mu_B} \int \mathrm{d}\boldsymbol{r} \exp(\mathrm{i}\boldsymbol{k} \cdot \boldsymbol{r})\,[M_S(\boldsymbol{r})\xi(\theta,\alpha) + M_L(\boldsymbol{r})\zeta(\theta,\alpha)]\end{aligned} \tag{2.10}$$

and the equality defines spin and orbital geometric factors ξ and ζ, respectively, that are convenient to use in subsequent developments.

It is useful to note that the geometric factors in (2.10) assume a quite simple form for the special case $\theta = \pi/2$. In this instance the quantity enclosed by the open-face brackets reduces to

$$M_S(\boldsymbol{r})[\sin\alpha + (\varepsilon/2)(\cos\alpha + \sin\alpha)] + \tfrac{1}{2}M_L(\boldsymbol{r})[\sin\alpha + (1+\varepsilon)\cos\alpha]. \tag{2.11}$$

The Compton limit of the contribution to the cross section made by (2.10) is derived in the following section.

3. The Compton limit

By the Compton limit of the cross section we mean the form achieved for high-energy incident photons and a large scattering vector. In this context it is useful to note that for $\theta = \pi/2$, $E = 45$ keV and $E' = 40$ keV we have $k = \sqrt{q^2 + q'^2} \simeq 30$ Å^{-1}.

We illustrate a method by which to extract the Compton limit of the polarisation-induced contribution to the cross section by reporting steps involved for the orbital part of (2.10). The arguments used can be applied to any contribution to the cross section but in the experiments reported only the interference term is measured. Returning to (2.1) and using (2.10) it is evident that we need to consider the limiting form of the

correlation function (if the momentum density is purely real, the correlation functions formed with n^+M and M^+n are identical)

$$\int_{-\infty}^{\infty} \frac{\mathrm{d}t}{2\pi\hbar} \exp(-\mathrm{i}\omega t) \langle n^+(\boldsymbol{k}) \int \mathrm{d}\boldsymbol{r} \exp(\mathrm{i}\boldsymbol{k}\cdot\boldsymbol{r})\, M_L(\boldsymbol{r}, t)\rangle. \tag{3.1}$$

The first step is to insert the explicit expression for the charge density (2.14) and the Heisenberg operator $M_L(\boldsymbol{r}, t)$ defined for the total electron Hamiltonian H. At the same time we insert $1 = \exp[\mathrm{i}\boldsymbol{k}\cdot(\boldsymbol{R}_j - \boldsymbol{R}_j)]$ to obtain the correlation function

$$\sum_j \left\langle [\exp(-\mathrm{i}\boldsymbol{k}\cdot\boldsymbol{R}_j) \exp\left(\frac{\mathrm{i}Ht}{\hbar}\right) \exp(\mathrm{i}\boldsymbol{k}\cdot\boldsymbol{R}_j)] \right.$$

$$\left. \times \int \mathrm{d}\boldsymbol{r} \exp[\mathrm{i}\boldsymbol{k}\cdot(\boldsymbol{r} - \boldsymbol{R}_j)]\, M_L(\boldsymbol{r}) \exp\left(\frac{-\mathrm{i}tH}{\hbar}\right)\right\rangle. \tag{3.2}$$

The effect of the similarity transformation on $\exp(\mathrm{i}Ht/\hbar)$ is to shift the momentum operator $\boldsymbol{p}_j$ in H by an amount $\hbar\boldsymbol{k}$; the transformed Hamiltonian is denoted by H'. From the invariance of the correlation function to a cyclic permutation of operators (3.2) is equal to

$$\sum_j \left\langle \exp\left(\frac{-\mathrm{i}Ht}{\hbar}\right) \exp\left(\frac{\mathrm{i}H't}{\hbar}\right) \int \mathrm{d}\boldsymbol{r} \exp[\mathrm{i}\boldsymbol{k}\cdot(\boldsymbol{r} - \boldsymbol{R}_j)] M_L(\boldsymbol{r}) \right\rangle. \tag{3.3}$$

Thus far we have just rearranged the correlation function (3.1). To pass to the Compton limit we introduce two approximations which are good for large E and k.

First, we combine the two exponential operators in (3.3) as if H and H' commute. The error involved can be shown to mean the neglect of the force on the jth electron generated by electron correlations and the ion potentials. This step is equivalent to invoking the impulse approximation which is believed to be good when E greatly exceeds electron binding energies. If the momentum operators in H only appear in the kinetic energy, i.e. relativistic terms are negligible, then

$$H' - H = (\hbar/2m^*)(\hbar k^2 + 2\boldsymbol{k}\cdot\boldsymbol{p}_j)$$

where m^* is the effective electron mass. We also introduce the momentum density distribution operator through the identity

$$1 = \hbar \int \mathrm{d}\boldsymbol{q}\, \delta(\hbar\boldsymbol{q} - \boldsymbol{p}_j)$$

in order to get

$$\exp\left(\frac{-\mathrm{i}Ht}{\hbar}\right) \exp\left(\frac{\mathrm{i}H't}{\hbar}\right) \simeq \exp\left(\frac{\mathrm{i}t(H' - H)}{\hbar}\right)$$

$$= \hbar \int \mathrm{d}\boldsymbol{q} \exp\left(\frac{\mathrm{i}t\hbar}{2m^*}(k^2 + 2\boldsymbol{k}\cdot\boldsymbol{q})\right) \delta(\hbar\boldsymbol{q} - \boldsymbol{p}_j). \tag{3.4}$$

The first factor will give the explicit time-dependent part of the correlation function in the Compton limit. Since it is not an operator the time Fourier transform in (3.1) can be completed, and it produces a delta function which expresses conservation of energy.

The second approximation we make to (3.3) stems from the large value of k in the Compton limit. In view of this, the spatial phase factor in (3.3) averages to zero unless

$\boldsymbol{r} = \boldsymbol{R}_j$. This is often referred to as the incoherent approximation. Invoking this and using (3.4) we find that the correlation function (3.1) reduces to the following form:

$$\frac{1}{n_0}\int \mathrm{d}\boldsymbol{q}\,\delta\left(\omega - \frac{\hbar}{2m^*}(k^2 + 2\boldsymbol{k}\cdot\boldsymbol{q})\right)\sum_j \langle\delta(\hbar\boldsymbol{q} - \boldsymbol{p}_j)M_L(\boldsymbol{R}_j)\rangle \tag{3.5}$$

where n_0 is the electron number density.

The static correlation function in (3.5) is assumed to factor into the product of the momentum density of the polarised electrons engaged in the magnetisation, and the unit-cell orbital magnetisation density, denoted by $\rho(\boldsymbol{q})$ and $\mu_B F_L$, respectively. It can be shown that the factorisation occurs for electrons in atomic orbitals or Wannier band states.

Turning now to the Compton limit of the spin contribution to the interference term, the argument is the same with M_L in (3.5) replaced by M_S. Factorisation of the static correlation function in this instance is reasonable if relativistic terms are negligible. The unit-cell spin density is defined as $\mu_B F_S$.

In the interpretation of scattering from polarised band electrons it is clear that the momentum density distributions in general differ for the spin and orbital contributions. For electrons in a single band the distributions are generated from $n(\boldsymbol{q}\uparrow) \pm n(\boldsymbol{q}\downarrow)$ where $n(\boldsymbol{q}\sigma)$ is the occupation function for the band labelled by the wavevector $\boldsymbol{q}$ and spin index σ. We have assumed that the difference is minimal, i.e. for a single-band model the majority spin band dominates. When this condition is not well satisfied our simple interpretation, which employs a factorisation and a common momentum distribution, is dubious. The secure route is to compare data with calculated values of the weighted momentum distributions, namely

$$\sum_j \langle\delta(\hbar\boldsymbol{q} - \boldsymbol{p}_j)M_L(\boldsymbol{R}_j)\rangle \qquad \sum_j \langle\delta(\hbar\boldsymbol{q} - \boldsymbol{p}_j)M_S(\boldsymbol{R}_j)\rangle.$$

From the analysis of data given in section 5 it seems that our simple theory is adequate especially because in this experiment the integral over the Compton profile, rather than its spectral distribution, is recorded.

Assembling our results, the Compton limit of the interference contribution to the cross section is, apart from a factor $r_e^2 E'/E$,

$$(1/n_0)[F_S\xi(\theta, \alpha) + F_L\zeta(\theta, \alpha)]J(k) \tag{3.6a}$$

in which the Compton profile of polarised electrons is

$$J(k) = \int \mathrm{d}\boldsymbol{q}\,\rho(\boldsymbol{q})\delta\left(\omega - \frac{\hbar}{2m^*}(k^2 + 2\boldsymbol{k}\cdot\boldsymbol{q})\right) \tag{3.6b}$$

and in the experiments reported below where the integrated Compton flux is recorded:

$$\int_{-\infty}^{+\infty} J(k_z)\,\mathrm{d}\omega = n_0.$$

The geometric factors ξ and ζ are defined through (2.10). These are dimensionless quantities, as also are F_S/n_0 and F_L/n_0. The form of (3.6), namely the Compton profile modulated by a magnetic structure factor, is in accord with the experimental findings, reported in section 5.

In a neutron diffraction experiment the results are usually presented in terms of a unit-cell magnetisation structure factor $F(\boldsymbol{k})$. This is related to F_S and F_L by $F(\boldsymbol{0}) =$

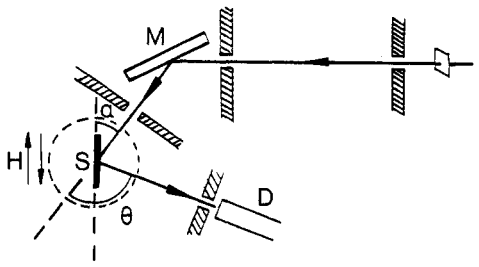

Figure 1. A schematic diagram of the experiment viewed from above. The white beam is extracted at about $\frac{1}{8}$ mrad above the orbital plane and monochromated by a plane Ge 111 crystal M. The sample S is clamped across the tapered poles of an iron-cored electromagnet which rotates about a vertical axis through the face of the sample and periodically reverses the field H. In these experiments θ, the scattering angle, was fixed and α was varied. The scattered radiation is recorded by D, a germanium semiconductor detector. The hatched areas denote collimators.

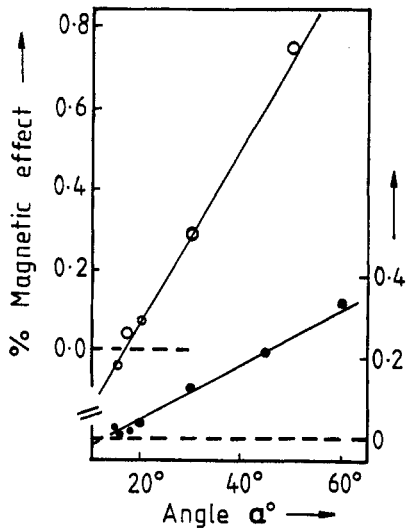

Figure 2. The measured fractional magnetic effect in iron (open circles) and cobalt (full circles), plotted against the angle α, defined in figure 1. The crossover angles α^* were obtained from a linear least-squares fit (full lines) over the angular ranges 15–30° and 15–45° for iron (left-hand ordinate) and cobalt (right-hand ordinate), respectively. The experimental errors in the magnetic modulation are roughly indicated by the size of the circles representing the data points.

$F_S + F_L$, which is a component of the diffraction pattern that is not accessible in a Bragg diffraction experiment, of course.

The structure factor $F_S\xi + F_L\zeta$ in (3.6) may vanish for a particular scattering geometry, as discussed in section 4. Given the values of $\zeta(\theta, \alpha)$ and $\xi(\theta, \alpha)$ for this geometry, obtained from a knowledge of the angles θ and α, we immediately find a value for the ratio F_L/F_S. For simple ferromagnets, with one atom per unit cell, F_L and F_S are proportional to the orbital and spin magnetic moments, and F_L/F_S is the ratio of the orbital to spin gyromagnetic factors.

For example, in 3d transition-metal magnets, in which the orbital moment is small and due largely to the spin–orbit interaction,

$$F_L/F_S = (g - 2)/2 \tag{3.7}$$

where g is the gyromagnetic factor. In the case of a rare-earth ion, characterised by spin, orbital and total angular momentum quantum numbers, S, L and J, respectively, the corresponding result is

$$F_L/F_S = g_L/g_S = [J(J+1) + L(L+1) - S(S+1)]/2[J(J+1) - L(L+1) + S(S+1)]. \tag{3.8}$$

Values of this ratio H_0^{3+} and S_m^{3+} ions, for example, are 1.5 and −1.2, respectively. In a ferrimagnet with a vanishingly small net moment it is not necessary for F_S and F_L to be individually equal to zero.

4. The experiment

A suitable test of the theory summarised in (3.6) is to measure values of θ and α where the magnetic structure factor vanishes and the scattered intensity is independent of the polarity of the applied field. From these angles the ratio F_L/F_S can be deduced. Two techniques are immediately apparent: either α can be fixed and the magnetic modulation measured as a function of θ, or vice versa. It turns out that the sensitivity of the two techniques is similar, so for simplicity the scattering angle was kept fixed.

Calculations show that over a fairly wide angular range around the zero or crossover point α^*, the fractional magnetic modulation is a linear function of the beam-to-magnetisation angle α to a very good approximation. Determination of α^* is therefore facilitated by a least-squares fit of the experimental data to a straight line. Since the experimental arrangement is similar to that adopted for magnetic Compton lineshape measurements (Collins *et al* 1989) it will be described only briefly here.

Radiation from the centre of the 5 T wiggler magnet at the Daresbury SRS was monochromated by a single Ge 111 reflection and scattered from a polycrystalline sample, clamped between the poles of an electromagnet (figure 1). The long thin shape of the sample ensured that the magnetisation direction was along its length. The beam-to-magnetisation angle α was adjusted by rotating the magnet–sample arrangement about a vertical axis. Scattered radiation was detected by a germanium solid state detector with a pre-detector slit to reduce the range of scattering angles observed. All observed scattering was in the horizontal plane. By raising the whole system by several millimetres the radiation source was viewed at some small angle above the orbital plane, thus using the 'inclined view' method to obtain a beam with a high degree of circular polarisation. The magnetic modulation, or fractional magnetic effect, was obtained by reversing the magnetising field direction in an asynchronous cycle and measuring the fractional change in Compton scattered intensity between the two field directions. One of the most important aspects of this technique of searching for a zero point in the magnetic modulation is that it is insensitive to systematic errors and completely independent of beam polarisation. The polarisation is therefore only important for optimisation of the experiment. Some experimental parameters are given in table 1.

The choice of scattering angle θ is very important. As the quantity of interest is the beam-to-magnetisation angle where the magnetic structure factor vanishes, θ should clearly be chosen so that this occurs within the range of accessible angles. Furthermore, some scattering angles give far greater sensitivity to F_L/F_S than others because both the precision to which α^* can be measured and the sensitivity of this angle to F_L/F_S are functions of θ. Calculations based on equation (3.6) and the known polarisation characteristics of the wiggler radiation (Laundy 1990, Collins *et al* 1990) indicate that, if F_L/F_S is small, as is the case for transition metals, a scattering angle of around 100° is appropriate. In this case, scattering in the horizontal plane is preferable because charge scattering of the dominant linearly polarised component is minimised. The ratio of magnetic to charge scattering is almost an order of magnitude higher than if a vertical scattering geometry had been adopted.

Table 1. Experimental parameters.

Incident bean energy	45 keV
Average scattered beam energy	40 keV
Scattered angle θ	98°
Monochromator bandpass	0.4 keV
Sample dimensions	50 mm × 8 mm × 1 mm
Source-to-monochromator distance	≃ 35 m
Incident beam width	2 mm
Incident beam height	6 mm
Height above or below axis	6 mm
Degree P_2 of circular polarisation	≃ 0.5
Degree P_3 of linear polarisation	≃ 0.8
Detector diameter	16 mm
Detector horizontal slit width	8 mm
Sample-to-detector distance	150 mm
Compton count rate	(1–4) × 10^4 s^{-1}
Field reversal period	2 s

Using the simple scattering table described, the absolute values of θ and α could not be determined to a precision of better than around 2°. This restriction was overcome by comparing the crossover angles for two samples of the same dimensions, as the difference in α^* can be determined precisely. Iron and cobalt polycrystals were chosen for the first measurements as they have large moments at room temperature and the ratios F_L/F_S are well known from independent g-factor measurements. A third sample, $HoFe_2$, was also measured as it was expected to have a large orbital moment at room temperature. The fractional magnetic effect in the Compton intensity was measured at various α angles, with many points repeated to check reproducibility. As a further test, some of the measurements were repeated by viewing the radiation source from below, rather than above, the orbital plane where the hand of polarisation is reversed. Data were collected for approximately 24 h for each of the three samples.

5. Experimental results

The data collected on iron and cobalt are presented in figure 2. It will be shown that these data agree very well with predictions. Data on the complex magnetic system $HoFe_2$ were of poorer statistical quality owing to high absorption and the smaller fraction of unpaired electrons. Despite the poorer quality of the data, some interesting departures from expected values were found. As these departures are not, as yet, fully understood, it is anticipated that $HoFe_2$ will form the subject of a separate communication. In this paper, only the cobalt and iron data will be analysed.

Useful information on the scattering system can be obtained both from the slope of the fractional magnetic effect against α, and from the value α^* where the line crosses zero. The slopes of the cobalt and iron data plots are different by a factor of about 3 owing to the different net moments induced in the samples. This is well understood by a comparison with magnetic induction measurements performed at room temperature with the same magnet and sample arrangement. Of far greater interest are the crossover

angles which were obtained from a linear least-squares fit of data near to the crossover points. The following angles were found:

$$\text{Fe: } \alpha^* = 16.3(3)^\circ \qquad \text{Co: } \alpha^* = 13.4(8)^\circ.$$

Since uncertainties in the scattering angle were around 2°, the difference between these two angles is of far greater significance than individual absolute values. A simple method of comparing the two crossover angles is to use the iron data to determine the scattering angle precisely and then compare the deduced value of F_L/F_S for cobalt with predictions.

For iron, $F_L/F_S = (g - 2)/2 = 0.046$ (Wohlfarth 1980). For the given crossover angle and beam energies a scattering angle θ of 98.30(15)° was predicted. This agrees very well with values of $\theta = 97(2)^\circ$ and 100(2)° measured geometrically and deduced from the Compton shift, respectively. Using this precise value for the scattering angle in the iron experiment, the ratio F_L/F_S for cobalt was calculated to be 0.107(18). This is in excellent agreement with the value of 0.094 obtained from independently measured g-factors.

6. Conclusions

We have shown that for magnetic Compton scattering the geometrical conditions for the vanishing of the magnetic structure factor can be related in a simple way to the ratio of orbital to spin moments in a ferromagnet. This has been confirmed from preliminary Compton measurements on iron and cobalt where the observed orbit-to-spin ratio is consistent with the independently determined g-factor. The technique is likely to be of most benefit to the study of systems with comparable spin and orbital moments, where the ratios are unknown and are unobtainable by other experimental methods. Such Compton measurements, which yield structure factors at $k = 0$, are complementary to technically difficult magnetic diffraction experiments where magnetic scattering at low momentum transfers is very weak. These data are more easily obtained, but require improved statistical precision.

Future theoretical work should include a study of the approximation employed in section 3. Of particular concern is the range of validity of the factorisation and use of a common distribution for the spin and orbital weighted momentum distributions. Note, however, that this source of uncertainty in the interpretation has been largely eliminated in this total scattering experiment by integrating over all scattered beam energies. It can therefore be shown that the total cross section evaluated with the incoherent approximation is proportional to the magnetic structure factor in equation (3.6*a*) provided it is safe to neglect the energy dependence of ξ and ζ. In our experiments the ω-dependence of these quantities is indeed very mild, and hence the average values of ξ and ζ can be used to a good approximation, namely ω equal to the Compton shift given in table 1. When such a procedure is justified it follows that the factorisation proposed in section 3 is consistent with the total cross section (often referred to as the static approximation) and this gives us added confidence in the factorisation.

Acknowledgments

We have benefited from discussions with Professor J B Forsyth, Professor B Johansson, Dr M Long and Dr A J Rollason. SPC and MJC are grateful to the Science and

Engineering Research Council for the provision of funding for synchrotron studies and to staff at the Daresbury Laboratory for their assistance.

References

Balcar E and Lovesey S W 1989 *Theory of Magnetic Neutron and Photon Scattering* (Oxford: Clarendon)
Collins S P, Cooper M J, Timms D N, Brahmia A, Laundy D and kane P P 1989 *J. Phys.: Condens. Matter* **1** 9009
Collins S P, Laundy D, Brahmia A, Timms D N, Jones S, Cooper M J and Rollason A 1990 *Nucl. Instrum. Methods* A **290** 254
Cooper M J 1987 *J. Physique Coll. Suppl.* 12 **48** C9 989
Cooper M J, Collins S P, Timms D N, Brahmia A, Kane P P, Holt R S and Laundy D 1988 *Nature* **333** 151
de Bergevin F and Brunel M 1986 *Structure and Dynamics of Molecular Systems* vol 2, ed R Daudel *et al* (Dordrecht: Reidel) p 69
Gibbs D, Harshman D R, Isaacs E D, McWhan D B, Mills D and Vettier C 1988 *Phys. Rev. Lett.* **61** 12417
Grotch H, Kazes E, Bhatt G and Owen D A 1983 *Phys. Rev.* A **27** 243
Laundy D 1990 *Nucl. Instrum. Methods* A **290** 248
Moon R M 1986 *Physica* A **137** 19
Wohlfarth E P 1980 *Ferromagnetic Materials* (Amsterdam: North-Holland) p 35